


Spin- $\frac{1}{2}$ string correlations and singlet-triplet gaps of frustrated ladders with ferromagnetic legs and alternate ferromagnetic and antiferromagnetic rungs

Monalisa Chatterjee,¹ Manoranjan Kumar,^{1,*} and Zoltán G. Soos^{2,†}

¹*S. N. Bose National Centre for Basic Sciences, Block-JD, Sector-III, Salt Lake, Kolkata 700106, India*

²*Department of Chemistry, Princeton University, Princeton, New Jersey 08544, USA*

 (Received 22 December 2023; revised 28 February 2024; accepted 5 March 2024; published 28 March 2024)

The frustrated ladder with alternate ferromagnetic exchange $-J_F$ and antiferromagnetic exchange J_A to first neighbors and ferromagnetic exchange $-J_L$ to second neighbors is studied by exact diagonalization and density matrix renormalization group calculations in systems of $2N$ spins- $\frac{1}{2}$ with periodic boundary conditions. The ground state is a singlet ($S = 0$) and the singlet-triplet gap ε_T is finite for the exchanges considered. Spin- $\frac{1}{2}$ string correlation functions $g_1(N)$ and $g_2(N)$ are defined for an even number N of consecutive spins in systems with two spins per unit cell; the ladder has string order $g_2(\infty) > 0$ and $g_1(\infty) = 0$. The minimum N^* of $g_2(N)$ is related to the range of ground-state spin correlations. Convergence to $g_2(\infty)$ is from below, and $g_1(N)$ decreases exponentially for $N \geq N^*$. Singlet valence bond (VB) diagrams account for the size dependencies. The frustrated ladder at special values of J_F , J_L , and J_A reduces to well-known models such as the spin-1 Heisenberg antiferromagnet and the J_1 - J_2 model, among others. Numerical analysis of ladders matches previous results for spin-1 gaps or string correlation functions and extends them to spin- $\frac{1}{2}$ systems. The nondegenerate singlet ground state of the ladder is a bond-order wave, a Kekulé VB diagram at $J_L = J_F/2 \leq J_A$, that is reversed on interchanging $-J_F$ and J_A . Inversion symmetry is spontaneously broken in the dimer phase of the J_1 - J_2 model where the Kekulé diagrams are the doubly degenerate ground states at $J_2/J_1 = 1/2$.

DOI: [10.1103/PhysRevB.109.094439](https://doi.org/10.1103/PhysRevB.109.094439)

I. INTRODUCTION

The spin- $\frac{1}{2}$ Heisenberg antiferromagnet (HAF) with isotropic AF exchange $J_1 > 0$ between first neighbors has been central to theoretical studies of correlated many-spin systems, including the famous exact 1D solution based on the Bethe ansatz [1] and the magnetism of inorganic [2] and organic [3] materials that contain 1D spin- $\frac{1}{2}$ chains. The addition of AF exchange $J_2 > 0$ between second neighbors introduces frustration and leads to interesting ground-state properties such as bond-order waves [4], spiral phases [5–7], and spin liquids [8] due to quantum fluctuations. The J_1 - J_2 model has been successfully applied to the magnetism of crystals with 1D chains of $S = \frac{1}{2}$ of transition metal ions such as Cu(II) [9,10].

Dimerized chains have lower symmetry and different J_1 with neighbors to the right and left. The AFAF model [11] has alternate $J_A = 1$ to one neighbor and variable $-J_F$ to the other. The model has attracted much attention since its approximate realization in some materials, e.g., $\text{Na}_2\text{Cu}_2\text{TeO}_6$ [12,13], CuNb_2O_6 [14], and $(\text{CH}_3)_2\text{NH}_2\text{CuCl}_3$ [15]. The AFAF model is the frustrated F-AF ladder in Fig. 1 with spin $S_r = \frac{1}{2}$ at site r and $J_L = 0$. The recent study [16] of weakly doped $\text{Sr}_{14}\text{Cu}_{24}\text{O}_{41}$ using resonant inelastic x-ray scattering illustrates the scope spin- $\frac{1}{2}$ ladders. Other two-leg ladder singlet ground states may exhibit superconductivity on tuning the exchange interactions [17–19].

The $J_F \rightarrow \infty$ limit of the AFAF model is the spin-1 HAF that has been intensively studied theoretically and numerically since Haldane predicted it to be gapped [20]. The ground state of the AFAF model with exchange $-J_L$ between second neighbors has interesting topological properties [21,22] as do AFAF models [22] with spins $S > \frac{1}{2}$, which are the focus of current research. The topological properties of AFAF models with $J_2 < 0$ pose open problems.

We study in this paper the F-AF ladder in Fig. 1 with three isotropic exchanges: F exchange $-J_L$ between neighbors $r, r + 2$ in legs, F exchange $-J_F$ at rungs $2r - 1, 2r$, and AF exchange J_A at rungs $2r, 2r + 1$. We consider parameters J_L, J_F and $J_A = 1$ leading to a singlet ($S = 0$) ground state $G(J_L, J_F)$. The ladder reduces to important models in special cases. These are the spin- $\frac{1}{2}$ HAF at $J_L = 0$ and $-J_F = J_A$ with one spin per unit cell and the AFAF model at $J_L = 0$ and $-J_F \neq J_A$ with two spins per unit cell. The ladder is frustrated except when $J_L = 0$ or $J_F = 0$. The limit $J_F \rightarrow \infty$ is the spin-1 HAF with $J = (1 - 2J_L)/4 > 0$ between adjacent F rungs. The limit $J_L \rightarrow \infty$ is a J_1 - J_2 model with $J_1 = (1 - J_F)/2 > 0$ and $J_2 = -J_L$. The symmetry is higher [23] at infinite J_F or J_L .

The spin Hamiltonian with $J_A = 1$ as the unit of energy is

$$H_{F-AF}(J_L, J_F) = \sum_{r=1}^N (\vec{S}_{2r} \cdot \vec{S}_{2r+1} - J_F \vec{S}_{2r-1} \cdot \vec{S}_{2r}) - J_L \sum_{r=1}^{2N} \vec{S}_r \cdot \vec{S}_{r+2}. \quad (1)$$

*manoranjan.kumar@bose.res.in

†soos@princeton.edu

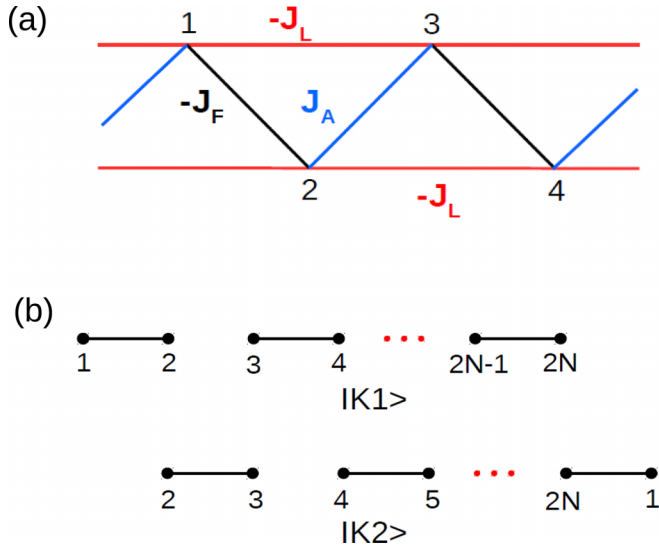


FIG. 1. (a) The F-AF spin- $\frac{1}{2}$ ladder with F exchange $-J_L < 0$ between spins r and $r+2$ in either leg, F exchange $-J_F$ in rungs $2r-1$, $2r$, and AF exchange J_A in rungs $2r$, $2r+1$. (b) Kekulé diagrams $|K1\rangle$ and $|K2\rangle$ with singlet-paired spins $(2r-1, 2r)$ and $(2r, 2r+1)$, $r = 1$ to N .

The total spin $S \leq N$ and its z component S^z are conserved. We consider systems of $2N$ spins with periodic boundary conditions and seek the thermodynamic limit $N \rightarrow \infty$. The ground state $G(J_L, J_F)$ in that limit has two noteworthy features. First, it is either a singlet or ferromagnetic [24] for any J_L, J_F and $J_A = 1$. Second, the exact $G(J_L, J_F)$ is a product of singlet-paired spins along a line where F exchanges cancel exactly. Both are central in the following. A product of singlet-paired spins is the exact ground state at special points of other 1D and 2D spin- $\frac{1}{2}$ systems [22,25–34].

We develop three themes. The first is string correlation functions in spin- $\frac{1}{2}$ chains. Den Nijs and Rommelse [35] and Tasaki [36] pointed out a hidden $Z_2 \times Z_2$ symmetry that can be measured by string correlation functions. Oshikawa [37] generalized the symmetry to Haldane chains with arbitrary integer $S > 1$. The critical theory of quantum spin chains by Affleck and Haldane [38] includes models with half-integer S and Z_2 symmetry. All the models considered [37,38] have equal isotropic exchange between either integer or half-integer S . The F-AF ladder has instead alternate $-J_F$ and $J_A = 1$ between first neighbors. It has two spins per unit cell in general, two string correlation functions, and Z_2 symmetry only in limits with one spin per unit cell.

The string correlation function $O(p-p')$ between consecutive spins from p to p' in the spin-1 HAF is finite in the limit $|p-p'| \rightarrow \infty$. Hida [11] adapted the spin-1 expression to string correlation functions of the AFAF model [$J_L = 0$ in Eq. (1)] with open boundary conditions. The string correlation functions $O(r-r')$ necessarily have an even number of consecutive spins- $\frac{1}{2}$ in Eq. (2) of Ref. [11].

We use this expression in general. The string correlation function for an even number N of consecutive spins- $\frac{1}{2}$ is

$$g_1(N) = \langle G | \exp \left(i\pi \sum_{j=1}^N S_j^z \right) | G \rangle. \quad (2)$$

The expectation value is with respect to the ground state in the thermodynamic limit or in finite systems with periodic boundary conditions. The general expression for spin- $\frac{1}{2}$ strings is well defined without reference to the spin-1 HAF. The initial spin is arbitrary in systems with one spin per unit cell. Since the F-AF ladder has two, the string correlation function $g_2(N)$ runs from $j = 2$ to $N+1$ in Eq. (2). In either case string correlation functions of $2p \leq 2N$ spins can be evaluated for $2N$ -spin ladders. The choice $2p = N$ is convenient for taking the thermodynamic limit.

The exact ground state along the line $J_L = J_F/2 \leq 1$ is the Kekulé valence bond (VB) diagram $|K2\rangle$ in Fig. 1 with singlet-paired spins $2r, 2r+1$ shown as lines, and as shown in Sec. IV, $g_2(N) = 1$, $g_1(N) = 0$ at any system size. To evaluate string correlation functions, we obtain the ground state $G(J_L, J_F, 2N)$ in increasingly large systems of $2N$ spins using exact diagonalization (ED) and density matrix renormalization group (DMRG) calculations. We interpret the results in terms of VB diagrams.

VB diagrams are an explicit general way to construct [39,40] correlated many-spin states in real space with conserved $S \leq N$ for $2N$ spins- $\frac{1}{2}$. The spins are placed at the vertices of the regular $2N$ polygon. A line (m, n) between vertices m and n represents normalized singlet-paired spins whose phase is fixed by $m < n$,

$$(m, n) = (\alpha_m \beta_n - \beta_m \alpha_n) / \sqrt{2}. \quad (3)$$

A legal (linearly independent) singlet diagram $|q\rangle$ has N lines (m, n) , an N -fold product of singlet-paired spins, that connects all $2N$ vertices once without any crossing lines. Diagrams with crossing lines are not linearly independent since they can be resolved into legal diagrams. The normalized singlet ground state is formally a linear combination of singlet diagrams,

$$|G(J_L, J_F, 2N)\rangle = \sum_q C(q, J_L, J_F) |q\rangle. \quad (4)$$

The sum is over $R_0(2N)$ singlet diagrams that depends only on system size. The coefficients $C(q, J_L, J_F)$ depend on models, parameters, and boundary conditions as well as system size. We find below the diagrams $|q\rangle$ that are eigenfunctions of the string operator in Eq. (2). The VB analysis accounts for the remarkable result of increasing string correlation functions $g_2(N)$ with system size. Convergence to string order $g_2(\infty)$ is from below.

The second theme is to recognize three regimes of the F-AF ladder in the positive quadrant of the J_L, J_F plane. Near the origin, in Eq. (1) is a system of N dimers with exchange $J_A = 1$ between spins $2r, 2r+1$, a singlet ground state, and frustrated F interactions between adjacent dimers. The singlet-triplet gap $\varepsilon_T(J_L, J_F)$ is large, spin correlations are short ranged, and small systems suffice for the thermodynamic limit. Increasing $J_F > 1$ while maintaining a singlet ground state leads to N rungs $2r-1, 2r$ with triplet ($S = 1$) ground states and net AF exchange $1 - 2J_L > 1$ between adjacent rungs. Increasing $J_L > 1$ while maintaining a singlet ground state leads to F legs with net AF exchange $1 - J_F > 0$ between spins in different legs. Results for general J_L, J_F are understood qualitatively this way.

The third theme is dimerization. The nondegenerate singlet ground state of Eq. (1) is a bond-order wave (BOW). The bond orders along the line $J_L = J_F/2 \leq 1$ are $\langle S_2 \cdot S_3 \rangle = -3/4$ for singlet-paired spins and $\langle S_1 \cdot S_2 \rangle = 0$ due to canceling F exchanges. Interchanging $-J_F$ and $J_A = 1$ reverses the BOW without changing the energy spectrum. Increasing J_F reduces the BOW to [23] $\langle S_1 \cdot S_2 \rangle = 1/4$ and $\langle S_2 \cdot S_3 \rangle = -0.350$ in the limit $J_F \rightarrow \infty$. Increasing J_L to infinity leads to $\langle S_1 \cdot S_2 \rangle = \langle S_2 \cdot S_3 \rangle = -1/4$ and suppresses dimerization.

We discuss F-AF ladders with parameters J_L, J_F in in Eq. (1) leading to singlet ground states. The paper is organized as follows. Section II summarizes the numerical methods used to obtain thermodynamic limits. Section III presents the singlet-triplet gap $\varepsilon_T(J_L, J_F)$ in the three regimes. String correlation functions $g_1(N)$ and $g_2(N)$ are defined in Sec. IV for spin- $\frac{1}{2}$ systems with two spins per unit cell. The $g_2(N)$ minimum at N^* is a collective estimate of the range of ground-state spin correlations, while $g_1(N)$ decreases exponentially with system size for $N \geq N^*$. In Sec. V we consider string correlation functions of the J_1 - J_2 model with one spin per unit cell and spontaneous dimerization for some parameters. Section VI is a brief summary.

II. METHODS

We use two numerical methods, ED and DMRG, to solve Eq. (1) at $J_A = 1$ and variable J_L, J_F in sectors with $S^z = 0$ or 1 for $2N$ spins- $\frac{1}{2}$ or for the HAF with n spins-1. ED up to 24 spins- $\frac{1}{2}$ is sufficient for the thermodynamic limit of systems with short-range correlations or large $\varepsilon_T(J_L, J_F)$. DMRG with periodic boundary conditions is used for larger systems. The ground state is a singlet when the lowest energy in the $S^z = 0$ sector does not appear in other sectors. We also perform VB calculations to obtain the coefficients $C(q)$ in Eq. (4) in systems of $2N \leq 16$ spins.

DMRG is a well-established numerical technique for the ground state and low-lying excited states of correlated 1D systems [41–43]. We use a modified DMRG algorithm that adds four new sites (instead of two) to the superblock at each step [44]. This avoids interaction terms between old blocks in models with second-neighbor exchange, here $-J_L$. All calculations are performed with periodic boundary conditions. We obtain truncation errors of 10^{-10} or less on keeping 512 eigenvectors of the density matrix and 4 or 5 finite sweeps. Systems up to $2N = 192$ spins- $\frac{1}{2}$ or $n = 64$ spins-1 were used for finite-size scaling.

There are additional external and internal checks on the accuracy of DMRG calculations. External checks are spin-1 calculations using other numerical methods [36,45] or DMRG with open boundary conditions [46]. Excellent agreement for spin correlation functions to 6 or 7 decimal places is due at least partly to the large Haldane gap [46] of the spin-1 HAF. Internal checks rely on the singlet/F boundary [24] at

$$J_F = 2J_L/(2J_L - 1), \quad 2J_L, J_F \geq 1. \quad (5)$$

The F energy per dimer is independent of system size,

$$\varepsilon_F(J_L, J_F) = -(2J_L + J_F - 1)/4. \quad (6)$$

The singlet ground state per dimer, $\varepsilon_0(J_L, J_F, 2N)$, is size dependent in general but must become size independent at

TABLE I. Ground-state energy ε_0 per dimer at constant J_+ and $J_- = \pm J_+$. ED at system sizes 16 and 24; the J_-^2 term of Eq. (7).

$J_+ = J_L$ $+J_F/2$	$J_- = J_L$ $-J_F/2$	$\varepsilon_0(16)$ $+3/4$	$\varepsilon_0(24)$ $+3/4$	J_-^2 term, Eq. (7)
0.4	0.4	-0.0486	-0.0486	-0.05
	-0.4	-0.0498	-0.0498	-0.05
0.8	0.8	-0.1604	-0.1599	-0.1714
	-0.8	-0.1679	-0.1678	-0.1714
1.2	1.2	-0.3069	-0.3046	-0.3375
	-1.2	-0.3220	-0.3217	-0.3375
1.6	1.6	-0.4742	-0.4695	-0.5333
	-1.6	-0.4945	-0.4939	-0.5333

the boundary. ED returns two states with $S^z = 0$ and one with $S^z = 1$ at $\varepsilon_0 = \varepsilon_F$. There are additional $S^z = 0$ and 1 states just above ε_F . The DMRG accuracy at $2N = 32$ drops to 4 or 5 decimal places for the dense spectrum at the boundary.

III. SINGLET-TRIPLET GAP

Near the origin of the J_L, J_F plane, the singlet ground state energy per dimer is conveniently written in terms of $J_{\pm} = J_L \pm J_F/2$,

$$\varepsilon_0(J_L, J_F) = -\frac{3}{4} - \frac{3J_-^2}{4(2+J_+)} + 0(J_-^3). \quad (7)$$

Spins $2r, 2r+1$ are dimers with exchange $J_A = 1$ and J_L, J_F cancel exactly when $J_- = 0$. The range of J_- at constant J_+ is from $-J_+$ at $(0, J_F)$ to J_+ at $(2J_L, 0)$. The ground state is a singlet for $J_+ \leq 2$, degenerate with $\varepsilon_F = -3/4$ at $J_L = 1, J_F = 2$. The virtual states at $(2+J_+)$ in second-order perturbation theory are singlet linear combinations of adjacent triplet dimers. ED results for $\varepsilon_0(J_L, J_F, 2N) + 3/4$ are listed in Table I for $2N = 16$ and 24 at constant J_+ and $J_- = \pm J_+$. The size dependence is weak. Differences at $J_- = \pm J_+$ are of order J_-^3 .

The upper panel of Fig. 2, shows $\varepsilon_T(J_L, J_F)$ at constant J_+ for $2N = 16$ and 24 as a function of $-J_+ \leq J_- \leq J_+$. The gap decreases from $\varepsilon_T(0, 0) = 1$ with increasing J_+ and is asymmetric in J_- . The size dependence is weak except at $J_+ = 2, J_- > 0$. The cusp at $J_- \approx 0$ and $J_+ = 0.4$ is due to lifting the N -fold degeneracy of localized triplets at $2r, 2r+1$. The lowest triplet is nondegenerate with wave vector $k = 0$ or π that switches from π to 0 with increasing J_- .

The lower panel of Fig. 2 zooms in on $\varepsilon_T(J_L, J_F, 2N)$ at $J_+ = 2.0$ and $-0.4 \leq J_- \leq 0.4$, which includes the singlet/F boundary at $J_- = 0$. The crossing points at positive and negative J_- are due to finite size. The singlet and F ground states are extensive while ε_T is intensive. In finite systems, the extensive difference $N(\varepsilon_F - \varepsilon_0)$ at the singlet/F boundary is a parabola, $-N$ times the J_-^2 term of Eq. (7). The calculated $\varepsilon_T(J_L, J_F, 2N)$ at $J_+ = 2, J_- = 0$ are $\varepsilon_T(20) = 0.0118, \varepsilon_T(24) = 0.0037$, and $\varepsilon_T(32) \approx 0.0031 \pm 0.001$. As mentioned in Sec. II, the dense spectrum at the boundary limits the numerical accuracy. The gaps of finite ladders in the lower panel are well approximated by parabolas with finite $\varepsilon_T \approx 0.003$ at $J_- = 0$, crossing points at $\varepsilon_T = N(\varepsilon_F - \varepsilon_0)$, and asymmetry due to J_-^3 .

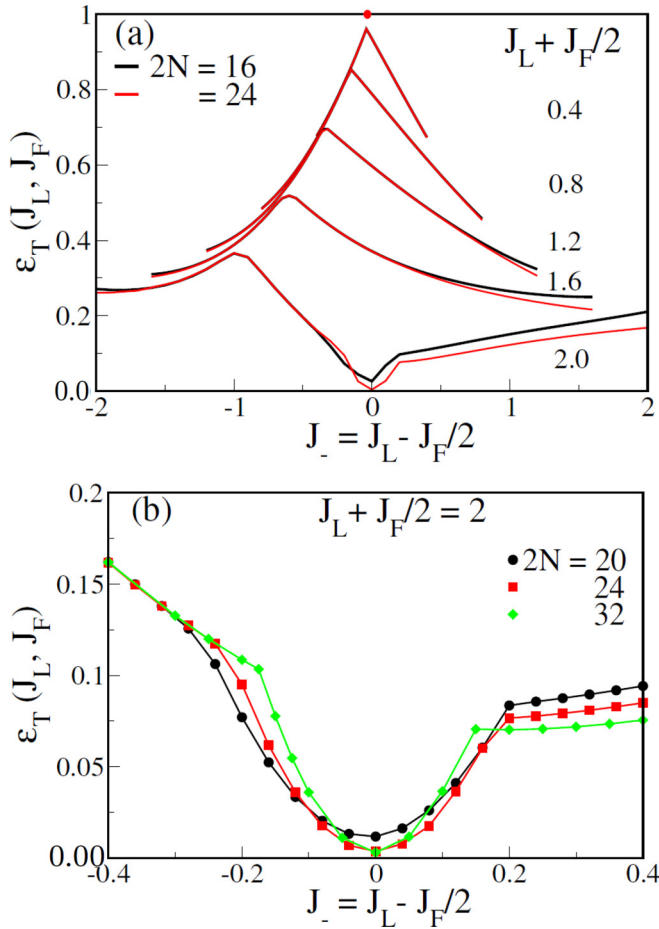


FIG. 2. (a) Singlet-triplet gap $\varepsilon_T(J_L, J_F)$ vs $J_- = J_L - J_F/2$ at constant $J_+ = J_L + J_F/2$ and system sizes $2N = 16$ and 24 . The range is $-J_+ \leq J_- \leq J_+$, and $\varepsilon_T(0, 0) = 1$. (b) $\varepsilon_T(J_L, J_F)$ at constant $J_+ = 2$ vs $-0.4 \leq J_- \leq 0.4$ at $2N = 20, 24$, and 32 . The crossing points are $\varepsilon_T = N(\varepsilon_F - \varepsilon_0)$.

The size dependence of $\varepsilon_T(J_L, J_F)$ is much weaker at $J_F > 2$ than at $J_L > 1$. In either case the singlet/F boundary, Eq. (5), limits the magnitude of the other exchange. Figure 3 shows $\varepsilon_T(J_L, J_F)$ at system sizes $2N = 16$ and 24 as a function of J_L at the indicated J_F . The maximum gap decreases and broadens with increasing J_F where triplets with different wave vectors are closely spaced. The $k = 0$ triplet is lowest when the gap is decreasing and (almost) vanishes at the singlet/F boundary. The $k = \pi$ triplets at $J_L = 0$ have the strongest size dependence.

The spins $2r - 1, 2r$ form triplets when J_F is large; the ground-state degeneracy is 3^N at $J_A = J_L = 0$. To study the large- J_F regime of the ladder, we rewrite Eq. (1) as

$$\begin{aligned}
 H_{F-AF}(J_L, J_F) = & -J_F \sum_{r=1}^N \vec{S}_{2r-1} \cdot \vec{S}_{2r} + (1 - 2J_L)/4 \\
 & \times \sum_{r=1}^N (\vec{S}_{2r-1} + \vec{S}_{2r}) \cdot (\vec{S}_{2r+1} + \vec{S}_{2r+2}) + V'.
 \end{aligned}
 \quad (8)$$

The first term corresponds to noninteracting dimers with triplet ground states. The second term is the spin-1 HAF with

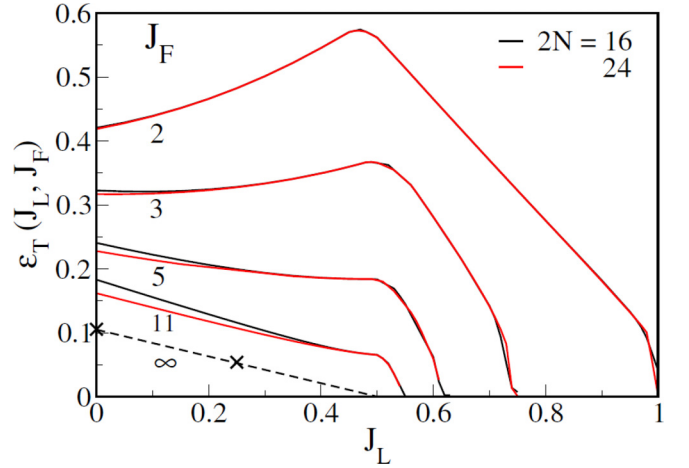


FIG. 3. Singlet-triplet gap $\varepsilon_T(J_L, J_F)$ vs J_L at constant J_F and system sizes $2N = 16$ and 24 . The gaps are < 0.005 at the singlet/F boundary, $2J_L = J_F/(J_F - 1)$. The dashed line is $(1 - 2J_L)\Delta(1)/4$ where $\Delta(1) = 0.4105$ is the Haldane gap [46]; the crosses at $J_L = 0$ and 0.25 are for $J_F = 200$ and $2N = 64$.

exchange $J = (1 - 2J_L)/4 > 0$ between neighboring rungs $2r, 2r - 1$. The operator V' contains all other exchanges. The coefficients are $(3 + 2J_L)/4$ for exchange between spins $2r, 2r + 1$; $-(1 + 2J_L)/4$ for exchange between spins r and $r + 2$; and $-(1 - 2J_L)/4$ for exchange between spins $2r - 1$ and $2r + 3$. Virtual excitations at finite J_F lead to effective Hamiltonians with excitations of order $1/J_F$. Equation (8) adiabatically connects ladders with finite J_F and $2J_L < 1$ to the spin-1 HAF with $V' = 0$ in the limit $J_F \rightarrow \infty$.

DMRG with open boundary conditions returns [46] $\Delta(1) = 0.4105$ for the Haldane gap. We find $\Delta(1) = 0.4106$ for 48 spins-1 and periodic boundary conditions. The dashed line in Fig. 3 is $(1 - 2J_L)\Delta(1)/4$. The gaps indicated by crosses at $J_L = 0$ and $1/2$ are 0.1055 and 0.0538 , respectively, at $J_F = 200$ and system size $2N = 64$.

The size dependence of $\varepsilon_T(J_L, J_F)$ is shown in Fig. 4 at constant $J_L = 1.5$, variable J_F in the upper panel and at constant $J_F = 1.5$, variable J_L in the lower panel. The singlet/F boundary is $(1.5, 1.5)$ where the estimated gap is < 0.005 . Both panels show $\varepsilon_T(J_L, J_F, 2N)$ minima in finite ladders and increasing gaps with weak size dependence at $(1.5, 1.45)$ or $(1.45, 1.5)$. The dashed lines are $1/N$ extrapolations. The remarkably small gap in Fig. 4(a) has been noted [21] previously using DMRG with open boundary conditions. Small $\varepsilon_T(J_L, J_F)$ with a minimum are found at $J_A = 1$ and comparable J_L, J_F with $J_L + J_F \approx 2.8$. We do not have an explanation for a minimum gap.

Figure 5 shows the J_L dependence of $\varepsilon_T(J_L, J_F)$ for the indicated J_F at $2N = 16$ and 24 in the upper and lower panels, respectively. The ladder with $-J_F = 1$ in Eq. (1) is a J_1 - J_2 model with $J_1 = 1$ and $J_2 = -J_L$. Ladders with other J_F have two spins per unit cell and correspond to alternating J_1 - J_2 models with $J_1 = (1 - J_F)/2$ and alternation $\pm(1 + J_F)/2$. Since the J_1 - J_2 model has noninteracting legs at $J_1 = 0$, the gap at $J_F = 1$ is entirely due to alternation. The gaps at $J_F = 0$ and $1/2$ in Fig. 5 are equal at $1/J_L = 0$. As expected, alternating exchanges increase the gap when J_L is finite.

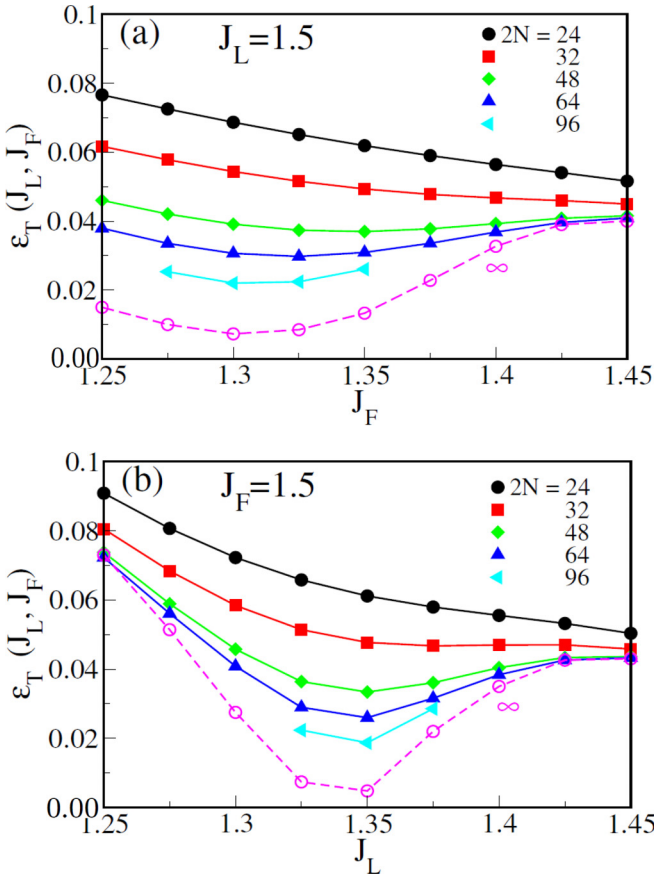


FIG. 4. Size dependence of singlet-triplet gaps $\varepsilon_T(J_L, J_F)$ at (a) constant $J_L = 1.5$, variable J_F and (b) constant $J_F = 1.5$, variable J_L . The dashed line is the $1/N$ extrapolation from $2N = 24$ to $2N = 64$ or 96 .

Equation (1) conserves total S but not the spins $S_A = S_B \leq N/2$ of each leg. Equal J' between all spins in different legs leads to separately conserved S , S_A , and S_B . Angular momentum addition returns $\varepsilon_T = J'$ when $J' > 0$. The mean-field approximation for $-J_F$ and $J_A = 1$ is $J' = (1 - J_F)/N$. The same result holds for the J_1 - J_2 model with $2N$ exchanges $J_1 = (1 - J_F)/2$. In the limit $J_L \rightarrow \infty$, the gap at system size $2N$ is

$$\varepsilon_T(J_F, 2N) = (1 - J_F)/N, \quad J_F \leq 1, J_L \rightarrow \infty. \quad (9)$$

Equation (9) agrees quantitatively with the numerical results at $1/J_L = 0$ in Fig. 5 for ladders and J_1 - J_2 models. Alternation increases ε_T .

The mean-field approximation has apparently not been recognized in systems with F exchange $-J_L$ in legs. The ladder with $J_F = 0$ and $J_A > 0$ in Fig. 1 has been studied numerically [47] and field-theoretically [48]. The F state is unconditionally unstable when $J_A > 0$, as expected on general grounds; it can be stabilized [47,48] by an Ising contribution to the isotropic exchange $-J_L$. Equation (9) is consistent with general expectations and provides quantitative gaps for finite ladders with $-J_F \leq 1$ in Eq. (1). The mean-field $\varepsilon_T(J_F, 2N)$ is elementary at $1/J_L = 0$ and rigorously decreases as $1/N$. It is a good approximation to at least $1/J_L = 0.1$.

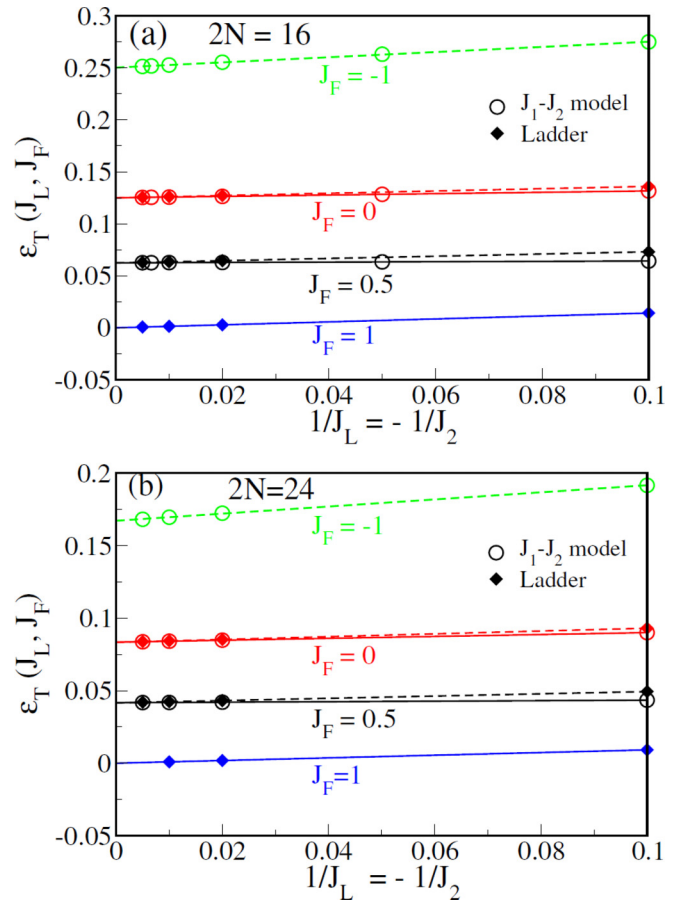


FIG. 5. Singlet-triplet gaps $\varepsilon_T(J_L, J_F)$ vs $1/J_L = -1/J_2$ at constant $J_F = -1, 0, 0.5$, and 1 at system sizes $2N = 16$ in (a) and 24 in (b). Open symbols refer to J_1 - J_2 models with $J_1 = (1 - J_F)/2$ and $J_2 = -J_F$. The ladder at $J_F = -1$ is a J_1 - J_2 model. The $1/J_L = 0$ gaps are $(1 - J_F)/2N$ for both. The $J_F = 1$ gap is finite in ladders, zero in J_1 - J_2 models.

We conclude this section by highlighting the difference between no net AF exchange and no exchange. The ladder at $J_F \rightarrow \infty$ is a spin-1 HAF with $J = (1 - 2J_L)/4$. The singlet/F boundary is at $J = 0$ where the energy per dimer is $\varepsilon_0 = \varepsilon_F = -J_F/4$. Since the boundary in Eq. (5) is at $2J_L > 1$ when J_F is finite, the ground state is a singlet at $1 - 2J_L = 0$ and no net exchange, with per dimer energy

$$\varepsilon_0(1/2, J_F)/J_F = -1/4 - c/J_F^2. \quad (10)$$

The first-order energy of Eq. (8) is zero at $2J_L = 1$. There is a second-order correction because $J_A = 1$ and $-J_L = 1/2$ are between different spins, $2r, 2r + 1$ for J_A and $r, r + 2$ for J_L . Equation (10) holds for $J_F > 10$ with $c = 0.516$ at both $2N = 16$ and 24 .

The $J_L \rightarrow \infty$ limit of the ladder is a J_1 - J_2 model. The singlet/F boundary is at $J_1 = 0$ with $\varepsilon_0 = -J_L/2$ when $J_F = 1$. The boundary of the ladder, $2J_L = J_F/(J_F - 1)$, is at $J_F > 1$ when J_L is finite. The ground state is a singlet at $J_F = 1$ and no net exchange between legs. But $\varepsilon_0(J_L, 1)$ has second-order corrections in $1/J_L$ since J_A and J_F are between different spins. We find $\varepsilon_0(J_L, 1)/J_L = -1/2 - d/J_L^2$ for $J_L > 10$ with $d = 0.271$ and 0.282 at $2N = 16$ and 24 .

IV. STRING CORRELATION FUNCTIONS

We obtain an explicit relation between spin-1 and spin- $\frac{1}{2}$ string correlation functions. Girvin and Arovas define [49] string correlation functions of consecutive $s = 1$ spins as

$$\tilde{g}(n) = -\left\langle s_1^z \left(\exp i\pi \sum_{j=2}^n s_j^z \right) s_{n+1}^z \right\rangle. \quad (11)$$

The expectation value is with respect to the singlet ground state in the thermodynamic limit or in finite chains with periodic boundary conditions. The $(n-1)$ spins-1 in the exponent can be written as $2(n-1)$ spins- $\frac{1}{2}$ with $s_j = S_{2j-1} + S_{2j}$. The other spins are $s_1 = S_1 + S_2$ and $s_{n+1} = S_{2n+1} + S_{2n+2}$. To have strings of consecutive spins- $\frac{1}{2}$, Hida [11] chose spins S_2 and S_{2n+1} and used the spin- $\frac{1}{2}$ identity,

$$-4S_m^z S_n^z = \exp i\pi (S_m^z + S_n^z), \quad (12)$$

to shift those spins into the exponent. This leads to $g_2(N)$ with N consecutive spins from 2 to $N+1$ in Eq. (2). As anticipated [11] on including the factor of 4, the string order $g_2(\infty)$ in the limit $J_F \rightarrow \infty$ is equal to $\tilde{g}(\infty)$.

The spin- $\frac{1}{2}$ string correlation function defined in Eq. (2) is not limited to either $J_F \rightarrow \infty$ or $N \rightarrow \infty$. Systems with two spins per unit cell have two strings of N spins. The string $g_1(N)$ in Eq. (2) has $N/2$ exchanges $-J_F$ and $N/2 - 1$ exchanges $J_A = 1$ while $g_2(N)$ has $N/2$ exchanges J_A and $N/2 - 1$ exchanges $-J_F$. The size dependencies of $g_1(N)$ and $g_2(N)$ are very different.

The string operator $\hat{g}_1(N)$ has an even number N of consecutive spins from 1 to N . Singlet VB diagrams $|q\rangle$ in systems of $2N$ spins have N lines (m, n) that correspond to singlet-paired spins in Eq. (3). Repeated use of Eq. (12) leads to

$$\begin{aligned} \exp \left(i\pi \sum_{j=1}^N S_j^z \right) |q\rangle &= |q\rangle, \quad 1 \leq m, n \leq N, \\ &= |q\rangle_T, \quad \text{otherwise.} \end{aligned} \quad (13)$$

Diagrams $|q\rangle$ with $1 \leq m, n \leq N$ are eigenfunctions with unit eigenvalue. The factor of 4 in Eq. (12) is required for normalization, $\langle q|q\rangle = 1$. The eigenfunctions are all possible singlets based on spins in the string.

Diagrams $|q\rangle$ that are not eigenfunctions contain one or more pairs of bridging lines (m, n) with only one spin in the string. Then $\hat{g}_1(N)|q\rangle$ generates a diagram $|q\rangle_T$ with triplet-paired spins $(m, n)_T = (\alpha_m \beta_n + \beta_m \alpha_n)/\sqrt{2}$ at all bridging lines. Spin orthogonality ensures $\langle q|q\rangle_T = 0$ but finite $\langle q'|q\rangle_T$ is possible with other singlets $|q'\rangle$. The Appendix summarizes two general properties of singlet VB diagrams: overlaps and dimensions. Overlaps $S_{q'q} = \langle q'|q\rangle$ are needed to evaluate expectation values. $R_0(2N)$ in Table II is the number of singlet diagrams at system size $2N$. A string of N spins has $R_0(N)$ eigenfunctions, each $R_0(N)$ -fold degenerate, without any bridging lines. The relative number of diagrams with bridging lines increases with system size as indicated by the decreasing ratio $R_0(N)^2/R_0(2N)$ in Table II.

We compute the string correlation functions $g_2(N)$ and $g_1(N)$ of the F-AF ladder with $2N$ spins Eq. (1). The upper panel of Fig. 6 shows the size dependence of $g_2(N)$ as $1/(2N)$

TABLE II. $R_0(2N)$ is the number of singlet VB diagrams for $2N$ spins. $R_0(N)$ is the number of eigenstates of an N -spin string. Equation (A4) is Stirling's approximation.

$2N$	$R_0(2N)$	$R_0(N)$	$R_0(N)^2/R_0(2N)$	Eq. (A4)
12	132	5	0.189	0.199
16	1430	14	0.137	0.143
20	16796	42	0.105	0.109
24	208012	132	0.0838	0.0861

from $2N = 12$ to 144 at $J_L = 0$ and $J_F = 2, 5$, and 50. The lower panel shows $g_1(N)$ on a logarithmic scale. At any system size, $g_2(J_F)$ is larger than $g_1(J_F)$ and decreases with J_F while $g_1(J_F)$ increases with J_F . Although not evident on the scale of Fig. 6, $g_2(N)$ at $J_F = 2$ increases from 0.789978 at $2N = 12$ and extrapolates to $g_2(\infty) = 0.794918$. At $J_F = 5$ and 50, $g_2(N)$ has a shallow minimum at $N^* = 8$ and 12, respectively. Convergence to $g_2(\infty)$ is again from below.

The following statements summarize results for other parameters J_L, J_F . String correlation functions satisfy the inequality

$$1 \geq g_2(N) > g_1(N) \geq 0. \quad (14)$$

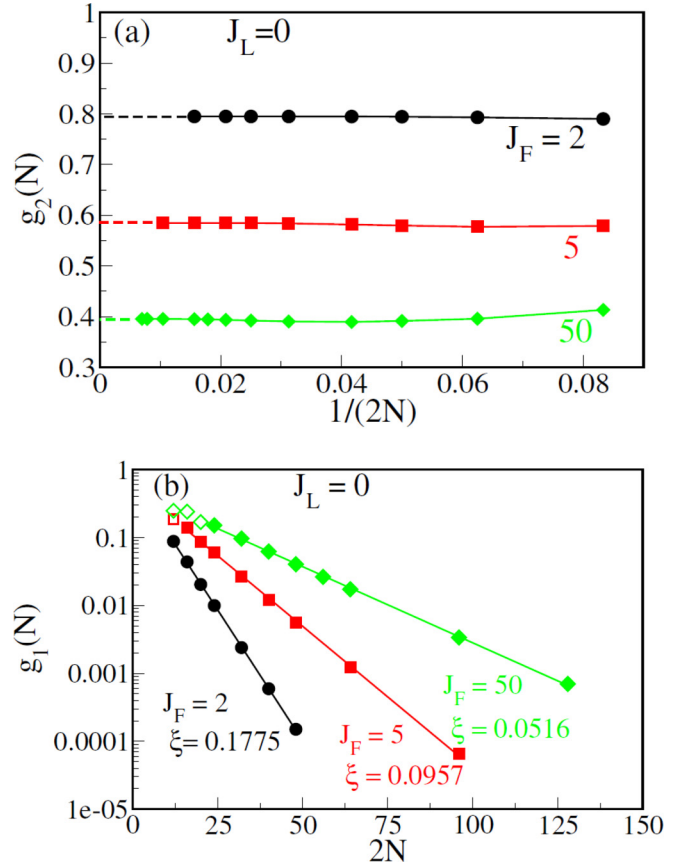


FIG. 6. (a) String correlation functions $g_2(N)$ at system size $2N$, $J_L = 0$, and $J_F = 2, 5$, and 50; linear extrapolation to string order $g_2(\infty)$. (b) $g_1(N)$ for the same J_L, J_F with solid symbols for $N \geq N^*$, the minimum of $g_2(N)$, open symbols for $N < N^*$. The lines are Eq. (15) with the indicated ξ .

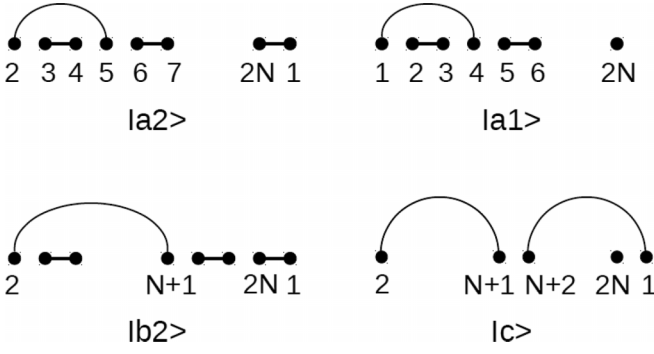


FIG. 7. Representative singlet VB diagrams $|q\rangle$ with N lines (m, n) in ladders with $2N$ spins and C_N translational symmetry: $|a2\rangle$ has one line $(2, 5)$ of length 3 and $(N - 1)$ lines of unit length; $|a1\rangle$ has one line $(1, 4)$ of length 3; $|b2\rangle$ has one line $(2, N + 1)$ of length $N - 1$, the maximum length; $|c\rangle$ has two lines of length $N - 1$, $(2, N + 1)$, and $(N + 2, 1)$.

The function $g_2(N)$ has a shallow minimum at system size $2N^*$. The size dependence of $g_1(N)$ is exponential for $N \geq N^*$,

$$g_1(N) = g_1(N^*) \exp[-2\xi(N - N^*)], \quad N \geq N^*. \quad (15)$$

The $g_2(N)$ minima in Fig. 6 are $N^* = 4, 8$, and 12 , respectively, for $J_F = 2, 5$, and 50 . The lines for $N \geq N^*$ in the lower panel are Eq. (15) with the indicated ξ .

We interpret $g_2(N)$ and $g_1(N)$ in terms of the VB ground state, Eq. (4), with coefficient $C(q)$ for diagram $|q\rangle$. The exact ground state is $|K2\rangle$ when $J_L = J_F/2 \leq 1$, with $C(K2) = 1$ and $C(q) = 0$ for all other $|q\rangle$. The expectation values are $g_2(N) = 1$ and $g_1(N) = 0$ independent of system size. The shortest string is $N = 4$ since consecutive spins return the spin correlation function $-4\langle S_1^z S_2^z \rangle$.

The ground state is a linear combination of singlet diagrams $|q\rangle$ when $|J_L - J_F/2| > 0$. The representative singlet VB diagrams $|q\rangle$ in Fig. 7 have N lines (m, n) ; lines not shown explicitly are between neighbors $(m, m + 1)$. The diagram $|a2\rangle$ differs from $|K2\rangle$ by two lines, $(2, 5)$ and $(3, 4)$. The N symmetry-related diagrams with a line $(2r, 2r + 3)$ have equal $C(q)$. The N diagrams $|a1\rangle$ in Fig. 7 with a line $(2r - 3, 2r)$ have equal $C(a1) < C(a2)$ since only line $(2, 3)$ is shared with $|K2\rangle$. Diagram $|b2\rangle$ has a line $(2r, 2r + N - 1)$ of length $N - 1$, the longest at system size $2N$. Diagram $|c\rangle$ has two lines of length $N - 1$ and $(N - 2)$ lines of unit length.

TABLE III. Ground-state coefficient $C(q)$ of diagrams $|q\rangle$ in Eq. (1) with $J_L = 0$, $J_F = 5$, and $2N$ spins. $|K1\rangle$ and $|K2\rangle$ are shown in Fig. 1, and $|a2\rangle$, $|a1\rangle$, $|b2\rangle$, and $|c\rangle$ in Fig. 7.

$C(q) \setminus 2N$	8	12	16
$C(K2)$	0.7583	0.6454	0.5607
$C(K1)$	0.1188	0.0217	0.0034
$C(a2)$	0.2981	0.2545	0.2213
$C(a1)$	0.0763	0.00556	0.00027
$C(b2)$	0.2981	0.0833	0.00045
$C(c)$	0.1172	0.0109	0.00144

Table III shows the size dependence of selected coefficients $C(q)$ at $J_L = 0$, $J_F = 5$. The strong decrease of $C(K1)$ with system size is due to the overlap $\langle K1|K2\rangle = (-2)^{-(N+1)}$. The decrease of $C(a1)$ is also due to overlap. As shown in the Appendix, diagrams $|q\rangle$ that differ from $|K2\rangle$ by a finite number of lines are asymptotically orthogonal to diagrams $|q'\rangle$ that differ from $|K1\rangle$ by a finite number of lines. The size dependence of $C(b2)$ illustrates the range of spin correlations, which is short at $J_L = 0$, $J_F = 5$, consistent with large $\varepsilon_T(0, 5)$ in Fig. 3. Diagram $|c\rangle$ has two lines of maximum length, and short-range spin correlations explain its size dependence.

Turning to string correlation functions, we note that $(N - 2)$ of the diagrams $|a2\rangle$ are eigenfunctions of $\hat{g}_2(N)$ while two diagrams have bridging lines, either $(2N, 3)(1, 2)$ or $(N, N + 3)(N + 1, N + 2)$. The relative number of bridging lines in $|a2\rangle$ decreases with system size. On the other hand, only two diagrams $|b2\rangle$ are eigenfunctions of $\hat{g}_2(N)$; the other $(N - 2)$ have bridging lines. As seen in Table II, the relative number of diagrams with bridging lines increases with system size, and so do their coefficients $C(q)$ for parameters J_L, J_F that increase the range of spin correlations.

Since the ladder is gapped, spin correlations are finite-ranged and $C(q)$ must be small for diagrams with lines (m, n) that exceed the range. We suppose N^* to be an estimate of the range. Then $g_2(N)$ and $g_1(N)$ decrease with system size up to $2N^*$ because the bridging lines increase more rapidly than eigenstates in Table II. By hypothesis, $C(q)$ is negligible for diagrams with lines longer than N^* . Then $g_2(N)$ increases when $N > N^*$ because diagrams with lines shorter than N^* are only bridging at the ends of increasingly long strings. The range N^* limits finite $C(q)$ to diagrams that differ from $|K2\rangle$ by a specified number of lines. The exponential decrease of $g_1(N)$ for $N > N^*$ in Eq. (15) is consistent with the asymptotic orthogonality of diagrams such as $|a2\rangle$ and $|a1\rangle$ that differ from $|K2\rangle$ and $|K1\rangle$, respectively, by two lines. It follows that $g_1(\infty) = 0$ and that $C(q) = 0$ in the thermodynamic limit for the $R_0(2N)/2$ diagrams $|q\rangle$ whose squared overlap is larger with $|K1\rangle$ than with $|K2\rangle$.

The panels of Fig. 8 show the size dependence of $g_2(N)$ and $g_1(N)$ in ladders with $2N$ spins, $J_F = 0$, and $J_L = 1, 2$, and 3 . The $g_2(N)$ minima are $N^* = 4, 16$, and 48 for $J_L = 1, 2$, and 3 . Larger systems are required for accurate extrapolation of $g_2(N)$ at $J_L = 3$. The solid lines $g_1(N)$ in the lower panel are Eq. (15) with the indicated ξ .

Table IV lists the string order $g_2(\infty)$, the minimum N^* of $g_2(N)$, and the spin gap ε_T for representative parameters J_L, J_F . We recall that $g_2(\infty) = 1 = C(K2)$ when $J_L = J_F/2 \leq 1$ while ε_T decreases from 1 at the origin to ≈ 0.003 at the singlet/F boundary. A $g_2(N)$ minimum at N^* requires J_L, J_F that lead to significant $C(q)$ for diagrams $|q\rangle$ with lines (m, n) longer than 4, the shortest string. The first two entries at $|J_L - J_F/2| = 0.25$ have almost equal $g_2(\infty)$ but quite different gaps; $g_2(N)$ has a minimum at $2N = 8$ for the smaller ε_T but not for the larger one, and the coefficients $C(K2), C(a2)$ are by far the largest in either case. Systems with $N^* = 4$ or 8 in the table return $g_2(\infty) > 0.75$ or > 0.5 , respectively. The exponential decrease of $g_1(N)$ for $N \geq N^*$ in Figs. 6(b) and 8(b) starts around $g_1(N^*) \approx 0.1$. The interpretation is that $C(q)$ is small for diagrams with lines (m, n) longer than

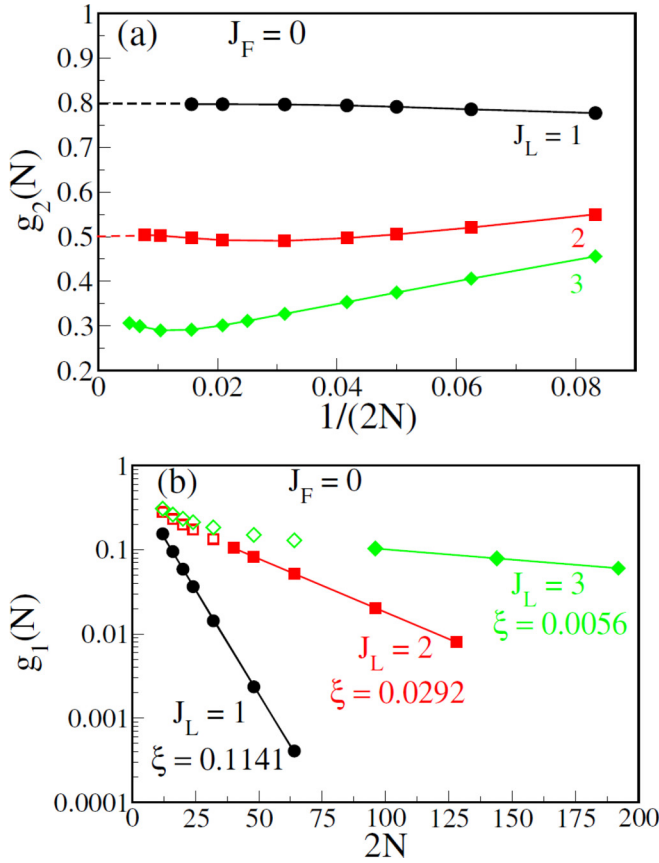


FIG. 8. (a) String correlation functions $g_2(N)$ at system size $2N$ and $J_F = 0$, $J_L = 1, 2$, and 3 . Linear extrapolation to string order $g_2(\infty)$. (b) $g_1(N)$ for the same J_L, J_F ; solid symbols for $N \geq N^*$, open symbols for $N < N^*$. The lines are Eq. (15) with the indicated ξ .

N^* . String order $g_2(\infty) < 0.25$ indicates longer-ranged spin correlations with $N^* > 50$ and gaps $\varepsilon_T < 0.1$.

The $g_2(N^*)$ minimum is exceptionally shallow at $J_L = 0.5$ and $J_F = 5$. Short-range correlations are to be expected at zero net exchange $1 - 2J_L$ between F rungs. We find con-

TABLE IV. String order $g_2(\infty)$, minimum N^* of $g_2(N)$, and gap ε_T in the thermodynamic limit for J_L, J_F in Eq. (1).

J_L	J_F	$g_2(\infty)$	N^*	ε_T
0.25	1	0.98144		0.777
1	1.5	0.98143	4	0.242
1	1	0.941	4	0.340
0.5	0	0.926	4	0.610
1	0	0.797	4	0.370
0	2	0.795	4	0.416
0.5	5	0.675	6	0.183
0.25	5	0.634	6	0.196
0	5	0.585	8	0.225
2	0	0.503	16	0.110
2	0.5	0.490	24	0.053
2	1	<0.09	>100	0.016
0	50	0.396	12	0.11
3	0	~0.31	48	0.038

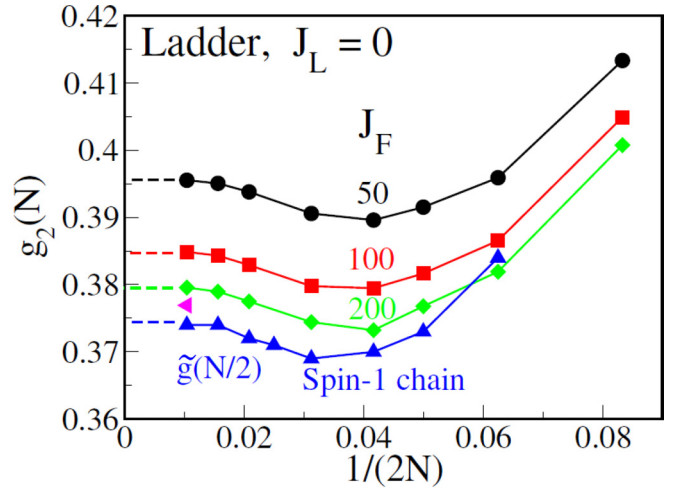


FIG. 9. Size dependence of $g_2(N)$ at $J_L = 0$ and the indicated J_F from $2N = 12$ to 96 . The string correlation function $\tilde{g}(N/2)$ is for the HAF with N spins-1. The magenta point at $2N = 96$ is for $J_F = 400$.

stant $g_2(N)$ for $N \geq N^*$ to three decimal places, very small $g_1(N^*) < 0.02$, and the only deviation from exponential behavior seen so far. Spin correlations at $J_F = 5$ in Table IV are shorter-ranged at $J_L = 0.5$ than at $J_L = 0$.

There is no net exchange between legs when $J_F = 1$. The $J_L = 2$ gaps in Table IV decrease from $J_F = 0$ to $J_F = 1$. In contrast to zero net exchange between rungs, however, N^* at $J_L = 2$ increases from 16 at $J_F = 0$ to 24 at $J_F = 0.5$ and exceeds 100 at $J_F = 1$. Longer ladders than $2N \approx 200$ will be required for $g_2(\infty) < 0.25$. For example, $g_2(N)$ is still decreasing at $2N = 192$ at $J_L = 1.5$, $J_F = 1.3$ or at $J_F = 1.5$, $J_L = 1.35$, the parameters with $\varepsilon_T < 0.01$ in Fig. 4.

We now turn to the $J_F \rightarrow \infty$ limit of the ladder, the spin-1 HAF with $J = 1/4$ at $J_L = 0$. Figure 9 compares the size dependence of $g_2(N)$ at system size $2N$, $J_L = 0$, and J_F with $\tilde{g}(N/2)$, Eq. (11), the string correlation function for N spins-1. Note the expanded scale. The string orders $\tilde{g}(\infty)$ and $g_2(\infty)$ are equal in the limit $J_F \rightarrow \infty$ by construction [11], as discussed above, but $g_2(N)$ is not equal to $\tilde{g}(N/2)$ at either finite J_F or finite N . The $\tilde{g}(N/2)$ minimum occurs at $N = 16$ spins-1. The string order is [46] $\tilde{g}(\infty) = 0.374325$ while we obtain $\tilde{g}(\infty) = 0.37427$ at 48 spins-1. We find $g_2(48) = 0.37692$ for 96 spins- $\frac{1}{2}$ and $J_F = 400$, and string order 0.37427 on linear extrapolation to $1/J_F = 0$.

The $\tilde{g}(N/2)$ minimum is a new result. Previous studies considered $\tilde{g}(p)$ at constant system size n and hence constant spin correlations with periodic [49] or open [46] boundary conditions; $\tilde{g}(p, n)$ decreases with p up to $n/2$ in small cyclic systems or to $\tilde{g}(\infty)$ as shown in Fig. 5 of Ref. [46]. The corresponding spin- $\frac{1}{2}$ function $g_2(2p, 2N)$ has variable p at constant system size $2N$, and it also decreases to $2p = N$ or to $g_2(\infty)$ in the thermodynamic limit. We have instead studied the size dependence of $g_2(N, 2N)$ and found an unanticipated minimum at N^* . Convergence to string order $g_2(\infty)$ is from below. The VB analysis rationalizes the size dependencies of both $g_2(N, 2N)$ and $\tilde{g}(n/2, n)$.

Finite string order $g_2(\infty)$ and gap ε_T are expected on general grounds in dimerized ladders with $-J_F \neq J_A$ and two spins per unit cell. The ground state is a BOW. The limit $J_F \rightarrow$

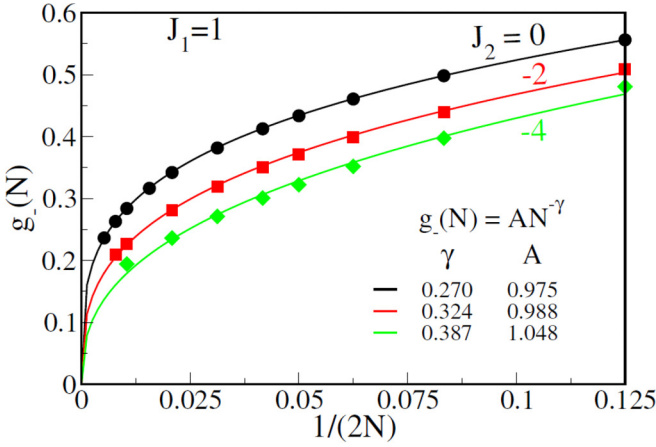


FIG. 10. Size dependence of the string correlation function $g_-(N)$ of J_1 - J_2 models with $2N$ spins, $J_1 = 1$, and $J_2 = 0, -2$, and -4 . The $J_2 = 0$ expression [11] is used at $J_2 = -2$ and -4 .

∞ generates inversion centers at the centers of rungs, and the ladder becomes a spin-1 HAF with $J = (1 - 2J_L)/4 > 0$ and Z_2 symmetry.

V. SPONTANEOUS DIMERIZATION

The F-AF ladder, Eq. (1), has two string correlation functions with an even number N of consecutive spins- $\frac{1}{2}$. The nondegenerate ground state is a BOW due to alternate first-neighbor exchanges $-J_F$ and $J_A = 1$. We set $-J_F = 1$ in this section and discuss the J_1 - J_2 model with $J_1 = 1$ and $J_2 = -J_L$. The model has one spin per unit cell, C_{2N} translational symmetry, and inversion symmetry σ at sites. The ground state for $2N$ spins, N even, is odd under inversion, $\sigma = -1$. The coefficients of $|K1\rangle$ and $|K2\rangle$ or of $|a2\rangle$ and $|a1\rangle$ in Table III are then equal with opposite sign. We have $C(q') \pm C(q)$ for symmetry-adapted linear combinations of singlets $|q\rangle$ and $|q'\rangle = \sigma|q\rangle$. The lowest singlet excited state has $\sigma = 1$ symmetry and $C(q') = C(q)$.

The string correlation function $g_-(N)$ is the ground-state expectation value. Hida [11] applied field theory to the spin- $\frac{1}{2}$ HAF ($J_2 = 0$) and concluded that $g_-(N)$ is proportional to $N^{-1/4}$, consistent with ED up to $2N = 24$. Figure 10 shows the size dependence of $g_-(N)$ at $J_2 = 0$ from $2N = 12$ to 192. The exponent $\gamma(0) = 0.270$ is the best fit, in good agreement with field theory. Since the model with $J_2 < 0$ is not frustrated, the size dependence of $g_-(N)$ at $J_2 = -2$ and -4 in Fig. 10 is also fitted as $AN^{-\gamma}$.

The J_1 - J_2 model is frustrated when $J_2 > 0$. The ground state is doubly degenerate in the dimer phase [50] $J_c = 0.2411 \leq J_2 \leq 1/2$. In finite systems, the singlets $\sigma = -1$ and $+1$ are the ground and first excited states, respectively. They are degenerate at $J_2 = 1/2$, the Majumdar-Ghosh point [25], where the exact $\sigma = \pm 1$ ground states are the plus and minus linear combinations of $|K1\rangle$ and $|K2\rangle$. The system is spontaneously dimerized.

The broken-symmetry state $|K2\rangle$ at $J_2 = 1/2$ returns $g_2(N) = 1$, $g_1(N) = 0$ as discussed for the ladder while $|K1\rangle$ has $g_1(N) = 1$, $g_2(N) = 0$. Due to overlaps, the string correlation functions $g_{\pm}(N)$ are size dependent. A straightforward

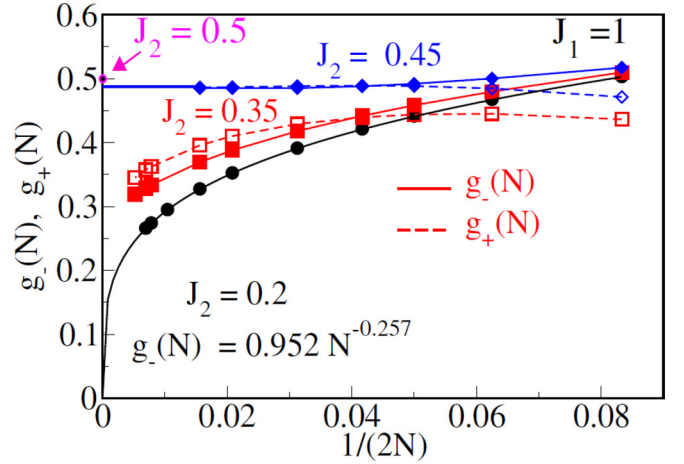


FIG. 11. String correlation function $g_-(N)$ at $J_2 = 0.2$ in the gapless phase, fitted as in Fig. 10. Solid and dashed lines are $g_-(N)$ and $g_+(N)$ at $J_2 = 0.35$ and 0.45 in the gapped dimer phase. The point at $J_2 = 0.5$ is exact. The lines at $J_2 = 0.35$ are to guide the eye.

calculation leads to

$$g_-(N) = 1/2 + 1/(2^N + 2). \quad (16)$$

The $g_+(N)$ expression has a minus signs in Eq. (16). Convergence to the thermodynamic limit is exponential.

Figure 11 shows the size dependence of $g_-(N)$ at $J_2 = 0.20 < J_c$ in the gapless phase and both string correlation functions at $J_2 = 0.45$ and 0.35 in the dimer phase. The $g_-(N)$ points at $J_2 = 0.20$ are fitted to $AN^{-\gamma}$ as in Fig. 10 with $\gamma = 0.257$. The point at 0.50 is exact for $J_2 = 0.5$. The $g_-(0.45, N)$ and $g_+(0.45, N)$ curves cross twice before converging to string order $g_-(\infty) = g_+(\infty) = 0.485$. Rapid size convergence and slightly reduced string order are expected close to $J_2 = 1/2$. We did not anticipate curve crossing; the ground state is odd under inversion at all system sizes.

The $J_2 = 0.35$ string correlation functions in Fig. 11 cross at system size $2N \approx 32$. The functions $g_+(N)$ and $g_-(N)$ are expected to have equal string order $g(\infty) > 0$. The difference $g_+(N) - g_-(N)$ increases to 0.029 at $2N = 144$ and decreases to 0.026 at $2N = 192$. Larger systems are required to evaluate the string order. The small gap $\varepsilon_T(1, 0.35) = 0.006$ also points to long but finite-ranged spin correlations.

VI. SUMMARY AND CONCLUSIONS

We have presented spin- $\frac{1}{2}$ string correlation functions and string order in general. The F-AF ladder, Eq. (1), at specific parameters J_L, J_F and $J_A = 1$ reduces to important spin- $\frac{1}{2}$ models with singlet ground states. It has two N -spin string correlation functions, $g_1(N)$ and $g_2(N)$, at system size $2N$, N even. Since the ladder is gapped, with $\varepsilon_T(J_L, J_F) > 0$ except in the limit $J_L \rightarrow \infty$, the string order is $g_2(\infty) > 0$, $g_1(\infty) = 0$. As shown in Fig. 9, the string order $g_2(\infty)$ in the limit $J_F \rightarrow \infty$ is equal to $\tilde{g}(\infty)$ of the spin-1 HAF, and the limits are approached from below.

The ground state near the origin of the J_L - J_F plane consists of rungs with AF exchange J_A that are weakly coupled by frustrated F exchanges $-J_L$ and $-J_F$ in Fig. 1. Short-range spin correlations are indicated by the gaps $\varepsilon_T(J_L, J_F)$ in Fig. 2,

by string order $g_2(\infty) > 3/4$, and by convergence to the thermodynamic limit at system size $2N = 24$. The regime $J_F > 3$, $J_L \leq 1/2$ has reduced $\varepsilon_T(J_L, J_F)$, finite $g_2(\infty)$, and spin correlations of intermediate range as indicated by the minimum N^* of $g_2(N)$. The regime $J_L > 2$, $J_F \leq 1$ has small $\varepsilon_T(J_L, J_F)$ that vanishes as $1/J_L$ in Fig. 4. The range of spin correlations is $N^* \approx 50$ at $J_L = 3$ and increases rapidly with J_L . The gapless J_1 - J_2 model with $J_2 = -J_L$ is the limit $J_L \rightarrow \infty$. The model is frustrated when $J_2 > 0$ and illustrates spontaneous dimerization in the dimer phase with finite ε_T and string order.

String correlation functions of the F-AF ladder directly probe ground-state spin correlations and their range. They afford more nuanced information than the binary choice of finite range in gapped systems and infinite range in gapless systems. The estimated range of spin correlations at J_L, J_F and $J_A = 1$ in Eq. (1) is N^* , the minimum of $g_2(N)$. The VB interpretation accounts for convergence to string order $g_2(\infty)$ from below and the exponential decrease of $g_1(N)$ for $N \geq N^*$. Ranges up to $N^* \sim 100$ are accessible in DMRG calculations up to system size $2N = 200$.

The spin-1 HAF has one spin-1 per unit cell and can be written in terms of two spins- $\frac{1}{2}$ as $s_j = S_{2j-1} + S_{2j}$ with F exchange $-J_F$ in rungs and AF exchange $J/4$ between adjacent rungs. There are now two spins per unit cell and $J_F \rightarrow \infty$ excludes singlet-paired rungs. In the VB treatment of finite spin-1 HAFs, Eq. (1) was expressed [51] in terms of spin- $\frac{1}{2}$ operators in a way that gave vanishing matrix elements for diagrams $|q\rangle$ with singlet-paired rungs $2j - 1, 2j$. F alignment in rungs clearly requires AF exchange and two spins per unit cell in order to have a singlet ground state.

ACKNOWLEDGMENTS

Z.G.S. thanks D. Huse for fruitful discussions. M.K. thanks SERB for financial support through Grant Sanction No. CRG/2020/000754. M.C. thanks DST-INSPIRE for financial support.

APPENDIX

We summarize the overlap of singlet VB diagrams and the size dependence of the singlet sector. In systems of $2N$ spins, singlet diagrams $|q\rangle$ have N lines (m, n) that correspond to normalized singlet-paired spins in Eq. (3) and connect the vertices of the $2N$ polygon without any crossing lines. The

overlaps are

$$S_{q'q} = \langle q'|q\rangle = (-2)^{-N+I(q',q)}. \quad (\text{A1})$$

$I(q', q)$ is the number of disconnected lines called islands by Pauling when the diagrams are superimposed. The superposition of any diagram with itself generates N islands of doubled lines (m, n) and unit overlap. The other extreme, illustrated by $\langle K1|K2\rangle = (-2)^{-N+1}$, is a single island for diagrams without any (m, n) in common. $I(q', q)$ is the number of shared lines (m, n) plus the number of islands with lines connecting vertices at unshared (m, n) . The Kekulé diagrams have no shared (m, n) ; their overlap of any $|q\rangle$ satisfies the relation

$$I(q, K1) + I(q, K2) = N + 1. \quad (\text{A2})$$

Overlap magnitudes are necessarily larger with one of the Kekulé diagrams when N is even, and overlap magnitude uniquely relates half of the diagrams to $|K1\rangle$, the other half to $|K2\rangle$. The Kekulé diagrams are orthogonal in the thermodynamic limit, as are diagrams that differ from either by a finite number of lines (m, n) .

All eigenfunctions $|q\rangle$ of the string operator $\hat{g}_1(N)$ in Eq. (13) have $1 \leq m, n \leq N$. All other $|q\rangle$ have one or more pairs of bridging lines (m, n) with only one end in the string 1 to N . Then $\hat{g}_1(N)|q\rangle$ generates triplet-paired spins $(m, n)_T = (\alpha_m\beta_n + \beta_m\alpha_n)/\sqrt{2}$ at all bridging lines. For example, $\hat{g}_1(N)|K2\rangle$ generates diagram $|K'\rangle$ with unchanged (m, n) except for two bridging lines that become $(2N, 1)_T$ and $(N, N+1)_T$. The overlap of diagrams with triplets is zero unless the triplets are in the same island, in which case $S_{qq'}$ is Eq. (A1). We have $\langle K'|K2\rangle = 0$ due to spin orthogonality and $\langle K'|K1\rangle = (-2)^{-N+1}$ since both triplets are in the same island.

The dimensions of the VB basis have long been known. The number of singlet diagrams in systems of $2N$ spins is

$$R_0(2N) = \frac{(2N)!}{N!(N+1)!}. \quad (\text{A3})$$

The string operator for N spins has $R_0(N)$ eigenfunctions $|q\rangle$ with $N/2$ lines in the string. The degeneracy of each is $R_0(N)$ since $|q\rangle$ also has $N/2$ lines with (m, n) not in the string. The ratio of eigenstates to the total number of singlets is, using Stirling's approximation,

$$\frac{R_0(N)^2}{R_0(2N)} \approx \frac{8e(N+1)^{N+3/2}}{\sqrt{\pi}(N+2)^{N+3}}. \quad (\text{A4})$$

-
- [1] H. A. Bethe, Zur theorie der metalle. I. Eigenwerte und eigenfunktionen der linearen atomkette, *Z. Phys.* **71**, 205 (1931).
- [2] L. J. de Jongh and A. R. Miedema, Experiments on simple magnetic model systems, *Adv. Phys.* **23**, 1 (1974).
- [3] J. S. Miller, editor, *Extended Linear Chain Compounds* (Plenum Press, New York, 1983), Vol. 3.
- [4] M. Kumar and Z. G. Soos, Spin-parity and broken symmetry in finite spin- $\frac{1}{2}$ chains with frustrated exchange: Quantum transition from high to low spin, *Phys. Rev. B* **85**, 144415 (2012).
- [5] S. R. White and I. Affleck, Dimerization and incommensurate spiral spin correlations in the zigzag spin chain: Analogies to the Kondo lattice, *Phys. Rev. B* **54**, 9862 (1996).
- [6] M. Kumar, S. Ramasesha, and Z. G. Soos, Bond-order wave phase, spin solitons, and thermodynamics of a frustrated linear spin- $\frac{1}{2}$ Heisenberg antiferromagnet, *Phys. Rev. B* **81**, 054413 (2010).
- [7] M. Kumar, A. Parvej, and Z. G. Soos, Level crossing, spin structure factor and quantum phases of the frustrated spin-1/2 chain with first and second neighbor exchange, *J. Phys.: Condens. Matter* **27**, 316001 (2015).
- [8] L. Savary and L. Balents, Quantum spin liquids: a review, *Rep. Prog. Phys.* **80**, 016502 (2017).
- [9] M. Hase, I. Terasaki, K. Uchinokura, M. Tokunaga, N. Miura, and H. Obara, Magnetic phase diagram of the

- spin-Peierls cuprate CuGeO_3 , *Phys. Rev. B* **48**, 9616 (1993).
- [10] S. K. Saha, M. S. Roy, M. Kumar, and Z. G. Soos, Modeling the spin-Peierls transition of spin- $\frac{1}{2}$ chains with correlated states: J_1 - J_2 model, CuGeO_3 , and $\text{TTF-CuS}_4\text{C}_4(\text{CF}_3)_4$, *Phys. Rev. B* **101**, 054411 (2020).
- [11] K. Hida, Crossover between the Haldane-gap phase and the dimer phase in the spin- $\frac{1}{2}$ alternating Heisenberg chain, *Phys. Rev. B* **45**, 2207 (1992).
- [12] L.-F. Lin, R. Soni, Y. Zhang, S. Gao, A. Moreo, G. Alvarez, A. D. Christianson, M. B. Stone, and E. Dagotto, Electronic structure, magnetic properties, and pairing tendencies of the copper-based honeycomb lattice $\text{Na}_2\text{Cu}_2\text{TeO}_6$, *Phys. Rev. B* **105**, 245113 (2022).
- [13] S. Gao, L.-F. Lin, A. F. May, B. K. Rai, Q. Zhang, E. Dagotto, A. D. Christianson, and M. B. Stone, Weakly coupled alternating $S = \frac{1}{2}$ chains in the distorted honeycomb lattice compound $\text{Na}_2\text{Cu}_2\text{TeO}_6$, *Phys. Rev. B* **102**, 220402(R) (2020).
- [14] K. Kodama, H. Harashina, H. Sasaki, M. Kato, M. Sato, K. Kakurai, and M. Nishi, Neutron scattering study on the quasi-one-dimensional spin-gap system CuNb_2O_6 , *J. Phys. Soc. Jpn.* **68**, 237 (1999).
- [15] M. B. Stone, W. Tian, M. D. Lumsden, G. E. Granroth, D. Mandrus, J.-H. Chung, N. Harrison, and S. E. Nagler, Quantum spin correlations in an organometallic alternating-sign chain, *Phys. Rev. Lett.* **99**, 087204 (2007).
- [16] Y. Tseng, E. Paris, K. P. Schmidt, W. Zhang, T. C. Asmara, R. Bag, V. N. Strocov, S. Singh, J. Schlappa, H. M. Rønnow *et al.*, Momentum-resolved spin-conserving two-triplon bound state and continuum in a cuprate ladder, *Commun. Phys.* **6**, 138 (2023).
- [17] E. Dagotto, J. Riera, and D. Scalapino, Superconductivity in ladders and coupled planes, *Phys. Rev. B* **45**, 5744(R) (1992).
- [18] N. D. Patel, A. Nocera, G. Alvarez, R. Arita, A. Moreo, and E. Dagotto, Magnetic properties and pairing tendencies of the iron-based superconducting ladder BaFe_2S_3 : Combined *ab initio* and density matrix renormalization group study, *Phys. Rev. B* **94**, 075119 (2016).
- [19] Y. Zhang, L. Lin, J.-J. Zhang, E. Dagotto, and S. Dong, Pressure-driven phase transition from antiferromagnetic semiconductor to nonmagnetic metal in the two-leg ladders AFe_2X_3 ($A = \text{Ba}, \text{K}; X = \text{S}, \text{Se}$), *Phys. Rev. B* **95**, 115154 (2017).
- [20] F. D. M. Haldane, Continuum dynamics of the 1-D Heisenberg antiferromagnet: Identification with the $O(3)$ nonlinear sigma model, *Phys. Lett. A* **93**, 464 (1983).
- [21] K. Hida, K. Takano, and H. Suzuki, Topological phases of the spin- $\frac{1}{2}$ ferromagnetic-antiferromagnetic alternating Heisenberg chain with frustrated next-nearest-neighbour interaction, *J. Phys. Soc. Jpn.* **82**, 064703 (2013).
- [22] S. Sahoo, D. Dey, S. K. Saha, and M. Kumar, Haldane and dimer phases in a frustrated spin chain: an exact groundstate and associated topological phase transition, *J. Phys.: Condens. Matter* **32**, 335601 (2020).
- [23] M. Chatterjee, M. Kumar, and Z. G. Soos, Singlet quantum phases of the frustrated spin- $\frac{1}{2}$ ladder with ferromagnetic (F) exchange in legs and alternating F-AF exchange in rungs, *Phys. Scr.* **99**, 025973 (2024).
- [24] D. V. Dmitriev, V. Ya. Krivnov, and A. A. Ovchinnikov, Exactly solvable spin ladder model with degenerate ferromagnetic and singlet states, *Eur. Phys. J. B* **14**, 91 (2000).
- [25] C. K. Majumdar and D. K. Ghosh, On next-nearest-neighbor interaction in linear chain. II, *J. Math. Phys.* **10**, 1399 (1969).
- [26] B. Sriram Shastry and B. Sutherland, Exact ground state of a quantum mechanical antiferromagnet, *Physica B+C* **108**, 1069 (1981).
- [27] S. Furukawa, T. Dodds, and Y. B. Kim, Ferromagnetically coupled dimers on the distorted Shastry-Sutherland lattice: Application to $(\text{CuCl})\text{LaNb}_2\text{O}_7$, *Phys. Rev. B* **84**, 054432 (2011).
- [28] S. R. White, Equivalence of the antiferromagnetic Heisenberg ladder to a single $S = 1$ chain, *Phys. Rev. B* **53**, 52 (1996).
- [29] B. Kumar, Quantum spin models with exact dimer ground states, *Phys. Rev. B* **66**, 024406 (2002).
- [30] T. Hong, L. Y. Zhu, X. Ke, V. O. Garlea, Y. Qiu, Y. Nambu, H. Yoshizawa, M. Zhu, G. E. Granroth, A. T. Savici, Z. Gai, and H. D. Zhou, Structural and magnetic properties in the quantum $S = \frac{1}{2}$ dimer system $\text{Ba}_3(\text{Cr}_{1-x}\text{V}_x)_2\text{O}_8$ with site disorder, *Phys. Rev. B* **87**, 144427 (2013).
- [31] A. A. Tsirlin, R. Nath, C. Geibel, and H. Rosner, Magnetic properties of $\text{Ag}_2\text{VOP}_2\text{O}_7$: An unexpected spin dimer system, *Phys. Rev. B* **77**, 104436 (2008).
- [32] P. Biswal, S. Guchhait, S. Ghosh, S. N. Sarangi, D. Samal, D. Swain, M. Kumar, and R. Nath, Crystal structure and magnetic properties of the spin- $\frac{1}{2}$ frustrated two-leg ladder compounds $(\text{C}_4\text{H}_{14}\text{N}_2)\text{Cu}_2\text{X}_6$ ($X = \text{Cl}$ and Br), *Phys. Rev. B* **108**, 134420 (2023).
- [33] R. Chitra, S. Pati, H. R. Krishnamurthy, D. Sen, and S. Ramasesha, Density-matrix renormalization-group studies of the spin- $\frac{1}{2}$ Heisenberg system with dimerization and frustration, *Phys. Rev. B* **52**, 6581 (1995).
- [34] C. Tassel, J. Kang, C. Lee, O. Hernandez, Y. Qiu, W. Paulus, E. Collet, B. Lake, T. Guidi, M.-H. Whangbo, C. Ritter, H. Kageyama, and S.-H. Lee, Ferromagnetically coupled Shastry-Sutherland quantum spin singlets in $(\text{CuCl})\text{LaNb}_2\text{O}_7$, *Phys. Rev. Lett.* **105**, 167205 (2010).
- [35] M. den Nijs and K. Rommelse, Preroughening transitions in crystal surfaces and valence-bond phases in quantum spin chains, *Phys. Rev. B* **40**, 4709 (1989).
- [36] T. Kennedy and H. Tasaki, Hidden symmetry breaking and the Haldane phase in $S = 1$ quantum spin chains, *Commun. Math. Phys.* **147**, 431 (1992).
- [37] M. Oshikawa, Hidden $Z_2 \times Z_2$ symmetry in quantum spin chains with arbitrary integer spin, *J. Phys.: Condens. Matter* **4**, 7469 (1992).
- [38] I. Affleck and F. D. M. Haldane, Critical theory of quantum spin chains, *Phys. Rev. B* **36**, 5291 (1987).
- [39] Z. G. Soos and S. Ramasesha, Valence-bond theory of linear Hubbard and Pariser-Parr-Pople models, *Phys. Rev. B* **29**, 5410 (1984).
- [40] S. Ramasesha and Z. G. Soos, Magnetic and optical properties of exact PPP states of naphthalene, *Chem. Phys.* **91**, 35 (1984).
- [41] S. R. White, Density matrix formulation for quantum renormalization groups, *Phys. Rev. Lett.* **69**, 2863 (1992).
- [42] U. Schollwöck, The density-matrix renormalization group, *Rev. Mod. Phys.* **77**, 259 (2005).
- [43] K. A. Hallberg, New trends in density matrix renormalization, *Adv. Phys.* **55**, 477 (2006).
- [44] S. K. Saha, D. Dey, M. Kumar, and Z. G. Soos, Hybrid exact diagonalization and density matrix renormalization group

- approach to the thermodynamics of one-dimensional quantum models, *Phys. Rev. B* **99**, 195144 (2019).
- [45] K. Nomura, Spin correlation function of the $S = 1$ antiferromagnetic Heisenberg chain by the large-cluster-decomposition Monte Carlo method, *Phys. Rev. B* **40**, 2421 (1989).
- [46] S. R. White and D. A. Huse, Numerical renormalization-group study of low-lying eigenstates of the antiferromagnetic $S = 1$ Heisenberg chain, *Phys. Rev. B* **48**, 3844 (1993).
- [47] M. Roji and S. Miyashita, Competition between classical ordered state and quantum state in ferromagnetic chains coupled by antiferromagnetic bonds, *J. Phys. Soc. Jpn.* **65**, 883 (1996).
- [48] A. K. Kolezhuk and H.-J. Mikeska, Phase transitions in the Heisenberg spin ladder with ferromagnetic legs, *Phys. Rev. B* **53**, R8848(R) (1996).
- [49] S. M. Girvin and D. P. Arovas, Hidden topological order in integer quantum spin chains, *Phys. Scr.* **1989**, 156 (1989).
- [50] Z. G. Soos, A. Parvej, and M. Kumar, Numerical study of incommensurate and decoupled phases of spin- $\frac{1}{2}$ chains with isotropic exchange J_1, J_2 between first and second neighbors, *J. Phys.: Condens. Matter* **28**, 175603 (2016).
- [51] K. Chang, I. Affleck, G. W. Hayden, and Z. G. Soos, A study of the bilinear-biquadratic spin-1 antiferromagnetic chain using the valence-bond basis, *J. Phys.: Condens. Matter* **1**, 153 (1989).